Catalysis Letters Vol. 106, Nos. 1–2, January 2006 (© 2006)
DOI: 10.1007/s10562-005-9190-7

Tailoring alumina support with crystalline $AlPO_4$-5 for enhancing hydrodesulfurization activity

Baojian Shen*, Huifeng Li, and Shikong Shen

State Key Laboratory of Heavy Oil Processing, The Key Laboratory of Catalysis of CNPC, and Faculty of Chemical Science and Engineering, China University of Petroleum-Beijing, Beijing Changping, 102249, China

Received 21 August 2005; accepted 6 October 2005

Crystalline $AlPO_4$-5 modified alumina was firstly developed as support for hydrodesulfurization (HDS). It can promote the reducibility of metal oxides, inhibit inactive nickel spinel formation and facilitate more polymeric tungsten species formation, which favors the promotion effect of nickel on tungsten and results in an enhanced activity in HDS of DBT.

KEY WORDS: crystalline $AlPO_4$-5; alumina; tailoring; composite support; metal-support interactions; hydrodesulfurization.

1. Introduction

Alumina is being used as support in most commercial hydrodesulfurization (HDS) catalysts, due to its outstanding textural and mechanical properties, and its ability to keep active metal phases highly dispersed and remain stable during operation or facilitate redispersion of them during regeneration [1,2]. But the strong interaction between alumina and metal species, is generally believed to be responsible for the formation of relatively less active "Type?" phases [1–3]. In order to adjust the strong metal-support interactions, many elements (Ti, Si, P, F, B, Mg, Na, etc.) have been tested as additives with the desire to modify the surface properties of alumina, such as changing its surface acidity [4,5] or its ability in accommodating the metals [6–10]. However, the tailoring effects of the framework elements of molecular sieves on alumina surface have never been seen in open literature.

Here we would like to report the first example of $AlPO_4$-5 modified alumina for HDS, prepared by incorporating crystalline $AlPO_4$-5 into the alumina matrix. Notably, the crystalline $AlPO_4$-5, characteristic of alternate tetrahedral aluminum and phosphorus atoms bridged by oxygen atoms [11], owns very mild acidity to avoid undesired cracking brought by acidic molecular sieves [12]. The purpose of the present work is to investigate the tailoring effects of the crystalline aluminophosphate framework of $AlPO_4$-5 on alumina and its influence on metal-support interactions and HDS activity.

* To whom correspondence should be addressed.
E-mail: baojian@cup.edu.cn

2. Experimental

2.1. Composite support preparation

A typical preparation procedure was as follows. Firstly, $AlPO_4$-5 was synthesized according to the hydrothermal crystallization method [11], followed by centrifugation, filtering, and washing thoroughly. Secondly, the filter cake was repulped in deionized water. And under vigorous stirring (10,000 rpm) the obtained suspension was added dropwise into the pseudo-boehmite sol, which was prepared with the commercial pseudo-boehmite powders peptized with 5 wt% nitric acid at room temperature for 8 h. Thirdly, the sol mixture was stirred vigorously in a water bath at 348 K until the mixture became viscous paste, then followed by extruding, drying, calcining at 823 K for 5 h. The obtained composite support was designated AAP, containing the phosphorous content of 9 wt% (calculated by P_2O_5). And pure Al_2O_3 support was prepared directly from the acidified pseudo-boehmite sol as the reference sample, correspondingly.

2.2. Catalyst preparation

The catalysts NiW/AAP and NiW/Al_2O_3 with the loading of 4 wt% NiO and 27 wt% WO_3, were prepared by pore volume co-impregnation method with an aqueous solution of nickel nitrate and ammonium metatungstate, respectively. Prior to use, the samples were dried overnight at 393 K and calcined at 823 K for 4 h.

2.3. Characterization

2.3.1. X-ray diffraction

X-ray diffraction patterns were recorded on a SHIMADZU-6000 diffractometer, using the Cu K_α

radiation at 40 kV and 30 mA with a scanning rate of 2°/min.

2.3.2. ^{31}P MAS NMR

All solid-state NMR experiments were performed using a 6 mm Pencil probehead on a wide-bore Varian Unity Inova-300 spectrometer, operating at 121.4 MHz, $\pi/2$ (1.8 μs) pulses, 160 scans and 15 s recycle delay using zirconia rotors of 6 mm outside diameter spinning at 7.0 KHz and room temperature. ^{31}P chemical shifts are quoted with respect to an external 85% aqueous solution of H_3PO_4.

2.3.3. N_2 physisorption

The surface area and pore volume of the samples were determined by N_2 physisorption using a Micromeritics ASAP 2020 automated system. Each sample was degassed at 623 K for 5 h prior to N_2 physisorption.

2.3.4. Infrared Spectroscopy

Acid sites and acid type distribution of the oxide form catalysts were determined by infrared spectroscopy (IR) of chemisorbed pyridine. All spectra were recorded on a MAGNA-IR560ESP Fourier-transform infrared spectrometer at a resolution of 0.35 cm^{-1}. The sample degas was carried out at 623 K and 10^{-3} Pa for 4 h prior to the adsorption of pyridine. IR spectra were recorded after subsequent evacuation at increasing temperatures from 473 to 623 K (1 h at each temperature).

2.3.5. Temperature-programmed desorption

NH_3-temperature-programmed desorption (TPD) of the supports and the oxide form catalysts was performed, respectively, by using Quantachrome Autosorb-1, equipped with a QUADSTAR 32-bit quadrupole mass spectrometer (QMS) 200 to monitor the exit gas. A sample of 0.20 g was charged in the quartz tube and heated at a rate of 10 K/min to 773 K for 30 min under N_2 flow before exposure to 100% NH_3 at 298 K for 30 min. The NH_3-TPD spectrum was recorded from 373 to 973 K at the heating rate of 10 K/min after removing weakly adsorbed NH_3 by heating the catalyst to 373 K under pure N_2 flow. The total flow rate of gas was fixed as 30 cm^3/min.

2.3.6. Temperature-programmed reduction

The temperature-programmed reduction (TPR) experiments of the oxide form catalysts were carried out on a Quantachrome Autosorb-1. Prior to the reduction, the catalyst sample in a quartz reactor was pretreated in an O_2 flow of 30 cm^3/min at 573 K for 3 h and cooled down to room temperature. Then the TPR experiment was run in a 10% H_2/Ar (by volume) flow of 30 cm^3/min, heating up to 1273 K at a rate of 5 K/min, with a Quantachrome Autosorb-1-C TCD controller to monitor the exit gas.

2.3.7. Diffuse reflectance spectra

Diffuse reflectance spectra (DRS) of the oxide form catalysts were recorded in the 350–800 nm range using corresponding support as reference on a Hitachi U-4100 Spectrophotometer.

2.3.8. Laser Raman spectra

Laser Raman spectra of the oxide form catalysts were recorded in the range of 200–1400 cm^{-1} under ambient conditions on a computer-controlled Renishaw microscopic confocal Raman spectrometer, model RM2000, using the 514.5 nm line from a Spectra Physics model 165 Ar ion laser as the exciting source. The spectra shift width was typically 1 cm^{-1}, and laser source powers at the sample were ca. 4.7 mW.

2.3.9. X-ray fluorescence spectroscopy

The contents of Ni, W, and P were determined on a ZSX100e X-Ray fluorescence analyzer.

2.3.10. Catalytic activity evaluation

The HDS of DBT was carried out in a continuous flow fixed-bed micro-reactor under the conditions: 4.0 MPa, 553 K, the catalyst loading of 0.60 g, 0.58 wt% DBT in decane as the model feed, the feed flow rate of 6.85 mL/h, H_2/Oil ratio of 500 v/v. The catalysts were presulfided *in situ* with the sulfiding feed of 10 vol% CS_2 in decane, 4.0 MPa and 573 K. After steady-state conditions were reached, the liquid effluents were periodically collected. And the total sulfur content in the feed (S_{feed}) and products ($S_{product}$) was measured by using a LC-4 coulometric sulfur analyzer. Finally, the HDS activity of DBT was calculated as follows:

$$\text{HDS conversion}(\%) = [(S_{feed} - S_{product})/S_{feed}] \times 100.$$

3. Results and discussion

3.1. X-ray diffraction

The XRD patterns of the calcined samples as shown in figure 1 indicate that composite support AAP exhibits all the characteristic peaks of $AlPO_4$-5, confirming its stable embedding in the alumina matrix. After the loading of nickel and tungsten, the characteristic peaks of $AlPO_4$-5 partly weaken, ascribed to the dilution effect or partial breakdown of crystalline $AlPO_4$-5 structure caused by the metal species [13]. But no visible metal oxides peaks are found in the XRD patterns of NiW/AAP or NiW/Al_2O_3.

3.2. ^{31}P MAS NMR

In order to investigate if there was an interface between crystalline $AlPO_4$-5 and alumina in the composite support AAP, through which exerting the tailoring effects of $AlPO_4$-5 on alumina, the ^{31}P MAS NMR

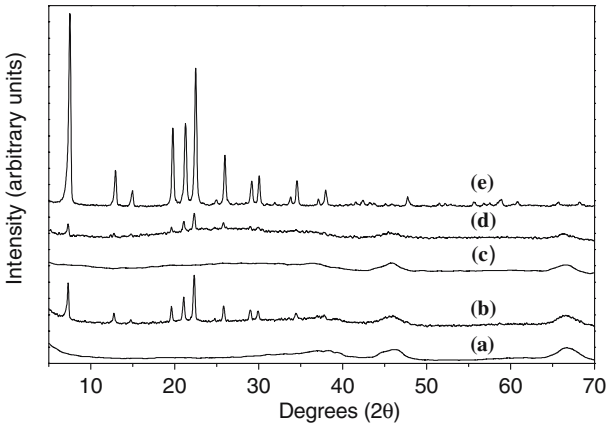

Figure 1. X-ray diffraction patterns of (a) Al_2O_3; (b) AAP; (c) NiW/Al_2O_3; (d) NiW/AAP and (e) $AlPO_4$-5.

spectra of $AlPO_4$-5 and composite support AAP were recorded, respectively. It can be clearly seen that there was a strong resonance at −29.3 ppm in the ^{31}P MAS NMR spectra of $AlPO_4$-5 (as shown in figure 2), which is characteristic of the tetrahedral phosphorus $P(OAl)_4$ in aluminophosphate molecular sieve $AlPO_4$-5 [14,15]. In contrast, a strong resonance at −29.4 ppm was also found in the ^{31}P MAS NMR spectra of composite support AAP (as shown in figure 3), which indicated that $AlPO_4$-5 is successfully stabilized in the alumina matrix and still retains its highly crystalline structure. Interestingly, a weak shoulder peak at −13.9 ppm was also found, suggesting that the chemical environment of some phosphorous atoms is different from the tetrahedral phosphorus $P(OAl)_4$ in molecular sieve $AlPO_4$-5 [14–16]. It can be reasonably explained that a new interface forms between molecular sieve $AlPO_4$-5 and alumina [17,18], because through our composite support preparation method, $AlPO_4$-5 was in close contact with alumina. Moreover, during the calcination treatment, the terminal hydroxyl groups on the outside surface of $AlPO_4$-5 particles maybe reacted with those of alumina surface to produce new chemical bonds.

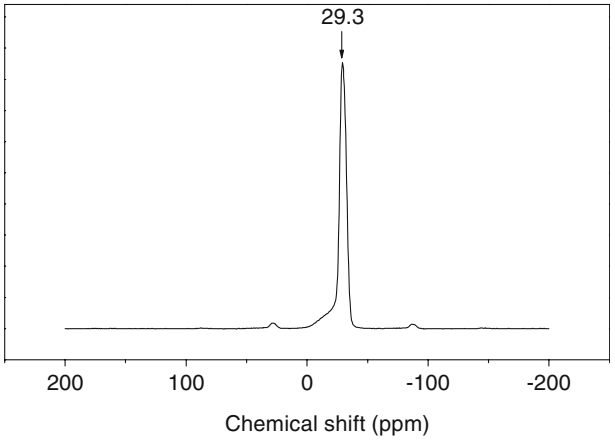

Figure 2. ^{31}P MAS NMR spectra of $AlPO_4$-5.

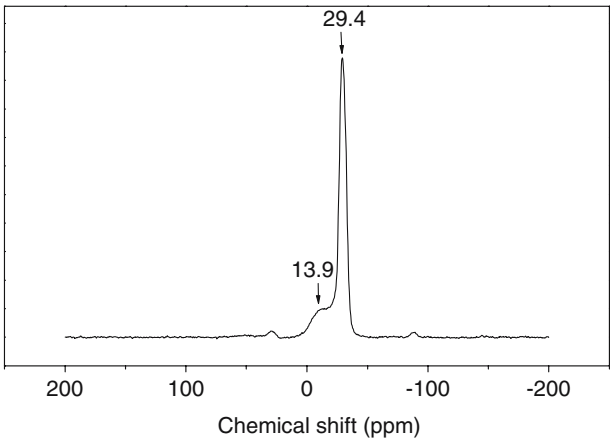

Figure 3. ^{31}P MAS NMR spectra of composite support AAP.

3.3. N_2 physisorption

The textural properties of the samples listed in table 1 indicate that the composite support AAP has larger surface area, but unexpectedly equivalent pore volume compared with pure alumina. It can be probably ascribed to a void space forming between $AlPO_4$-5 crystallites and alumina matrix, which contributes to the retained total pore volume [17,18]. However, after the loading of nickel and tungsten oxides, the surface area and pore volume of NiW/AAP decrease considerably and become smaller than those of NiW/Al_2O_3, due to partial blocking of the channels of $AlPO_4$-5 or breakdown of its crystalline structure caused by metal oxides [13].

3.4. Infrared spectroscopy

The results of the acid sites and acid type distribution of pure Al_2O_3 and $AlPO_4$-5 were shown in table 2. It is clear that $AlPO_4$-5 has less total acid sites (pyridine desorption temperature at 473 K) and less strong-strength acid sites (pyridine desorption temperature at 623 K), compared with Al_2O_3. In contrast, there are only L type acid sites on the alumina surface, while a few of both B type acid sites and L type acid sites are observed on the $AlPO_4$-5 surface, but such acid sites are mild and will not result in over-cracking as reported by the previous literature [19]. Moreover, it should be noted that no obvious signal of B type acid sites was observed

Table 1
BET surface areas and pore volumes of the samples

Sample	Surface area (m^2/g)	Pore volume (cm^3/g)
Al_2O_3	281	0.54
$AlPO_4$-5	309	0.12
AAP	293	0.54
NiW/Al_2O_3	193	0.36
NiW/AAP	180	0.34

Table 2
Total acid and acid type distribution of Al_2O_3 and $AlPO_4$-5

Sample	473 K		623 K	
	B acid (mmol/g)	L acid (mmol/g)	B acid (mmol/g)	L acid (mmol/g)
Al_2O_3	–	0.31	–	0.13
$AlPO_4$-5	0.022	0.058	0.011	0.031

in the pyridine-IR spectrum of composite support AAP, because of the dilution effect brought by alumina.

3.5. Temperature-programmed desorption

NH_3-TPD spectra of the supports and the oxide form catalysts were shown in figures 4 and 5, respectively. It is obvious that the shapes of the corresponding desorption curves of the supports Al_2O_3 and AAP or the catalysts NiW/Al_2O_3 and NiW/AAP are very analogous, suggesting similar acidity distributions over them. However, the NH_3 desorption peaks of both AAP and NiW/AAP shift to lower temperature slightly in comparison with those of Al_2O_3 and NiW/Al_2O_3, correspondingly, ascribed to that $AlPO_4$-5 owns less strong acid sites compared with Al_2O_3, which has been proven by the results of pyridine-IR desorption in table 2. The NH_3-TPD experimental results further confirm that NiW/AAP with the incorporation of $AlPO_4$-5 into alumina, unlike previously reported acidic molecular sieves [12], will not cause undesired over-cracking [19].

3.6. Temperature-programmed reduction

The TPR profiles of NiW/Al_2O_3 and NiW/AAP were shown in figure 6. It is evident that the TPR peaks of NiW/AAP notably shift to lower temperatures, compared with those of NiW/Al_2O_3, correspondingly. It can be properly interpreted that the incorporation of $AlPO_4$-5, especially attributed to the tailoring effects of its naturally $AlPO_4$-based framework, could play a beneficial role in suppressing the most reactive hydroxyl groups responsible for the metal oxides species interacting strongly with alumina support [20], due to their intimate contact and the formation of new interface, which has been confirmed by the characterization of ^{31}P MAS NMR. Furthermore, the introduction of $AlPO_4$-5 could also partly relieve the polarizing effect of aluminium ions of the alumina support on metal ions in the catalysts, which results in substantial improvement on metal-support interactions and causes easier reduction of nickel and tungsten species [7,8,20,21].

3.7. Diffuse reflectance spectra

The DRS spectra of NiW/Al_2O_3 and NiW/AAP were shown in figure 7. It is apparent that there are two peaks at 590 nm and 630 nm, characteristics of tetrahedrally coordinated Ni^{2+} ions in $NiAl_2O_4$, in the spectra of

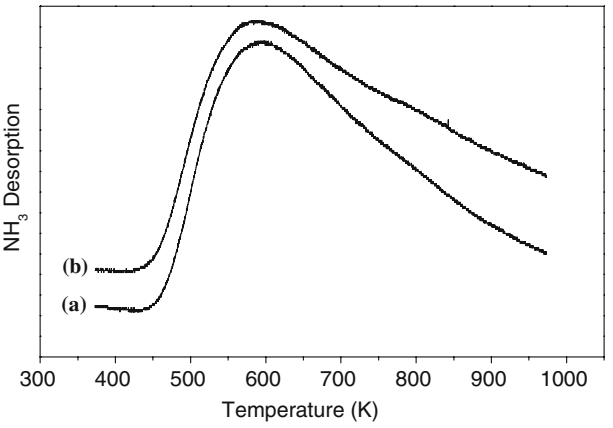

Figure 5. NH_3-TPD spectra of (a) NiW/AAP and (b) NiW/Al_2O_3.

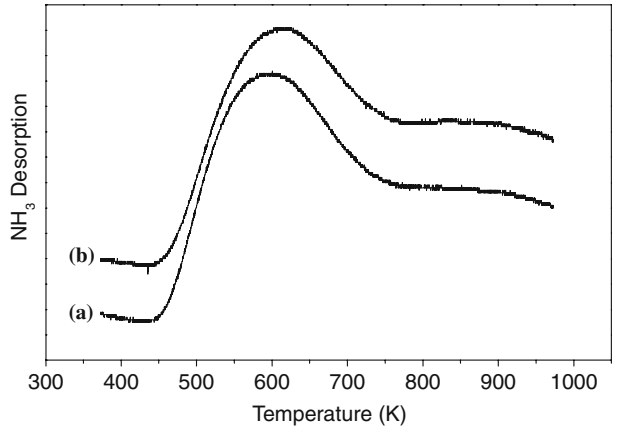

Figure 4. NH_3-TPD spectra of (a) AAP and (b) Al_2O_3.

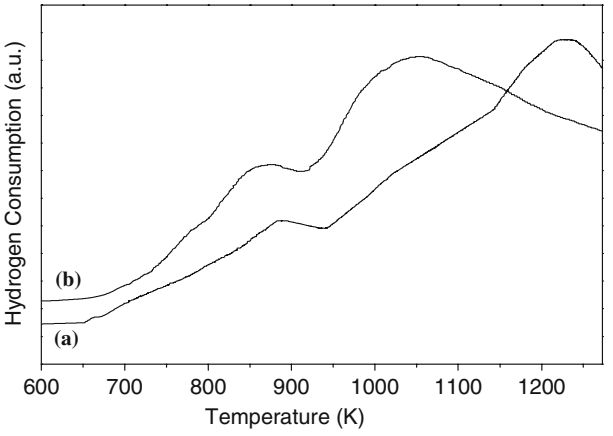

Figure 6. TPR profiles for (a) NiW/Al_2O_3 and (b) NiW/AAP.

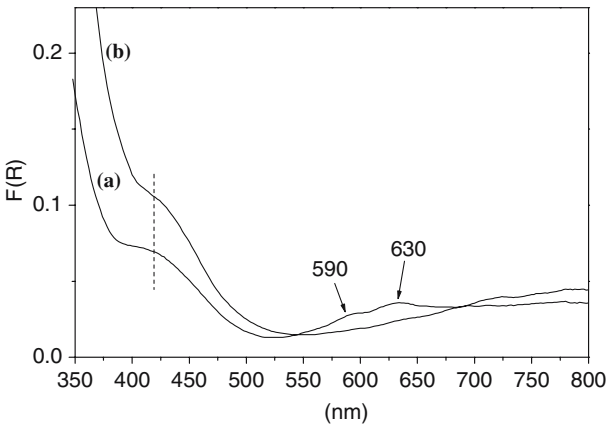

Figure 7. DRS spectra of (a) NiW/Al_2O_3 and (b) NiW/AAP.

NiW/Al_2O_3, agreeing well with the previous reports [22,23]. However, with the incorporation of $AlPO_4$-5 into alumina, such visible peaks disappear. Moreover, the band around 420 nm, characteristic of octahedrally coordinated Ni^{2+} ions, shifts to higher wavenumbers indicating an increased incorporation of nickel with tungsten producing Ni–W–O species [22,23]. Consequently, it is safe to conclude that the tailoring effects of aluminophosphate framework of $AlPO_4$-5 on alumina, can, to some extent, impede the diffusion of Ni ions into the alumina lattice [22,23], and facilitate the Ni^{2+} ions to be octahedrally coordinated on the composite support AAP.

3.8. Laser Raman spectra

The LR spectra of NiW/Al_2O_3 and NiW/AAP were shown in figure 8. In the LR spectra of NiW/Al_2O_3, a noticeable band at 975 cm^{-1} was found. However, the corresponding peak shifted to 979 cm^{-1} in the LR spectra of NiW/AAP, indicating that with the incorporation of $AlPO_4$-5, the degree of polymerization of tungsten species is increased [24–26]. It could be attributed to the surface properties of composite support AAP favoring the formation of octahedrally coordinated polymeric tungsten species, which has been reported to interact with support weakly, contributing to easier reducibility (as confirmed by TPR experimental results in figure 6) and higher activity [24–27].

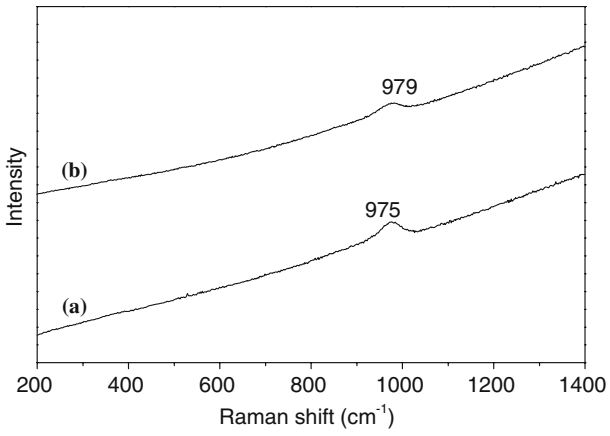

Figure 8. Laser Raman spectra of (a) NiW/Al_2O_3 and (b) NiW/AAP.

3.9. Catalytic activity evaluation

The HDS of DBT results were illustrated in figure 9. It indicates that NiW/AAP exhibits higher HDS activity, owning an increase of more than 5% in HDS conversion, compared with NiW/Al_2O_3. Furthermore, the compounds distribution of the liquid effluents obtained over NiW/AAP shows no obvious difference from that of NiW/Al_2O_3 according to the GC chromatograms, without much over-cracking products formation, due to its mild acidity as confirmed by the experimental results of Py-IR and NH_3-TPD.

Consequently, the remarkable increase in HDS activity of NiW/AAP can be ascribed to the reasons as follows. Firstly, the tailoring effects of $AlPO_4$-5 on alumina through the interface formed between them (as proven by ^{31}P MAS NMR spectra in figure 3) remarkably improve metal-support interactions and cause easier reduction of metal species (as illustrated in TPR profiles in figure 6); Secondly, the inhibiting formation of inactive nickel spinel (as confirmed by DRS spectra in figure 7), favors the promotion effect of nickel on tungsten; Thirdly, the increased degree of polymerization of tungsten species (as characterized by LR spectra in figure 8), according to the previous reports [6,27], maybe promoted the formation of the precursor of active sites (Ni–W–S species) for HDS.

4. Conclusion

NiW/AAP shows notably higher activity in HDS of DBT than NiW/Al_2O_3. It can be attributed to the advantages stemming from the tailoring effects of crystalline $AlPO_4$-5 on alumina. Firstly, the introduction of

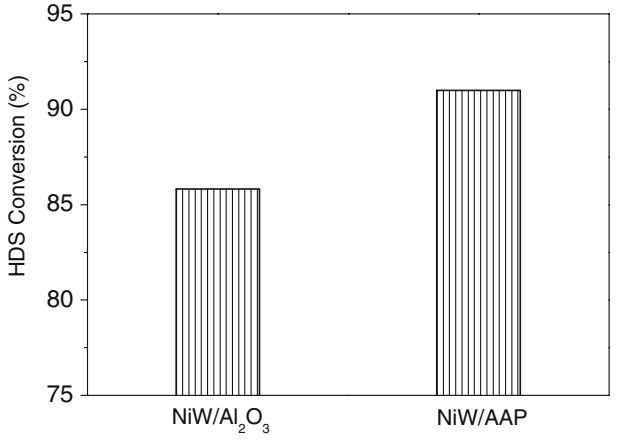

Figure 9. Comparison of the HDS activities of NiW/Al_2O_3 and NiW/AAP.

$AlPO_4$-5 into alumina substantially enhances the reducibility of metal oxides. Secondly, the inhibiting formation of inactive nickel spinel and the increased degree of polymerization of tungsten species, probably favored the promotion effect of nickel on tungsten or the formation of the precursor of active sites for HDS, resulting in a marked increase in HDS activity.

Acknowledgments

The authors gratefully acknowledge the funding of this project by PetroChina, NSFC (ID 20276039) and MOST "973" Project of China (2004CB217806).

References

[1] H. TopsØe, B.S. Clausen and F.E. Massoth, in: *Catalysis Science and Technology*, J.R. Anderson and M. Boudart (eds), Vol. 11 (Springer, Berlin, 1996) ch. 3.
[2] M. Breysse, P. Afanasiev, C. Geantet and M. Vrinat, Catal. Today 86 (2003) 5.
[3] S. Eijsbous, Appl. Catal. A 158 (1997) 53.
[4] D. Ferdous, A.K. Dalai and J. Adjaye, Appl. Catal. A 260 (2004) 137.
[5] D. Ferdous, A.K. Dalai and J. Adjaye, Appl. Catal. A 260 (2004) 153.
[6] C.J. Song, C. Kwak and S.H. Moon, Catal. Today 74 (2002) 193.
[7] T. Halachev, P. Atabasova, A. Lopez Agudo, M.G. Arias and J. Ramirez, Appl. Catal. A 136 (1996) 161.
[8] P. Atanasova, T. Tabakova, Ch. Vladov, T. Halachev and A. Lopez Agudo, Appl. Catal. A 161 (1997) 105.
[9] G.M. Dhar, B.N. Srinivas, M.S. Rana, M. Kumar and S.K. Maity, Catal. Today 86 (2003) 45.
[10] M. Sun, D. Nicosia and R. Prins, Catal. Today 86 (2003) 173.
[11] S.T. Wilson, Stud. Surf. Sci. Catal. 58 (1991) 137.
[12] G. Pérot, Catal. Today 86 (2003) 111.
[13] S. Bendezú, R. Cid, J.L.G. Fierro and A.L. Agudo, Appl. Catal. A 197 (2000) 47.
[14] A.M. Prakash, M. Hartmann and L. Kevan, Chem. Commun. (1997) 2221.
[15] C.S. Blackwell and R.L. Patton, J. Phys. Chem. 88 (1984) 6135.
[16] T.T.P. Cheung, K.W. Willcox, M.P. Mcdaniel and M.M. Johnson, J. Catal. 102 (1986) 10.
[17] Z.M.M. Noronha, J.L.F. Monteiro and P. Gélin, Micropor. Mesopor. Mat. 23 (1998) 331.
[18] M.V. Landau, D. Tavor, O. Regev, M.L. Kaliya and M. Herskowitz, Chem. Mater. 11 (1999) 2030.
[19] V.R. Choudhary and D.B. Akolekar, J. Catal. 103 (1987) 115.
[20] B. Scheffer, P. Molhoek and J.A. Moulijn, Appl. Catal. A 46 (1989) 11.
[21] L.J. Lakshmi, P.K. Rao, V.M. Mastikhin and A.V. Nosov, J. Phys. Chem. 97 (1993) 11,373.
[22] P. Atanasova and T. Halachev, Appl. Catal. A 108 (1994) 123.
[23] B. Scheffer, J.J. Heijeinga and J.A. Moulijin, J. Phys. Chem. 91 (1987) 4752.
[24] L. Salvati Jr., L.E. Makovsky, J.M. Stencel, F.R. Brown and D.M. Hercules, J. Phys. Chem. 85 (1981) 3700.
[25] A. Gutiérrez-Alejandre, J. Ramírez and G. Busca, Langmuir 14 (1998) 630.
[26] N. Kunisada, K.-H. Choi, Y. Korai, I. Mochida and K. Nakano, Appl. Catal. A 269 (2004) 43.
[27] D. Li, A. Nishijima, D.E. Morris and G.D. Guthrie, J. Catal. 188 (1999) 111.